Article

Pixel-Level Spatiotemporal Analyses of Vegetation Fractional Coverage Variation and Its Influential Factors in a Desert Steppe: A Case Study in Inner Mongolia, China

Yifan Song [1],*, Zhongxiao Guo [1], Yajing Lu [2], Denghua Yan [2], Zilong Liao [1], Huiwen Liu [3] and Yingjie Cui [1]

[1]   State Key Laboratory of Simulation and Regulation of Water Cycle in River Basin,
      Department of Water Resources for Pastoral Area, China Institute of Water Resources and Hydropower
      Research, Hohhot 010020, China; guozx@iwhr.com (Z.G.); liaozl@iwhr.com (Z.L.); cuiyj@iwhr.com (Y.C.)
[2]   State Key Laboratory of Simulation and Regulation of Water Cycle in River Basin,
      China Institute of Water Resources and Hydropower Research, Beijing 100038, China;
      luciaharry@163.com (Y.L.); yandh1006@163.com (D.Y.)
[3]   Power China Beijing Engineering Corporation Limited, Beijing 100024, China; liuhuiwen1224@163.com
*   Correspondence: songyf_90@163.com; Tel.: +86-159-470-37365

Abstract: Determining vegetation variation and its influential factors in a desert steppe under the impacts of climate change and human activities is crucial and meaningful for improving the understanding of desertification and taking targeted measures in ecological restoration. As compared to a large spatial scale such as a region or a whole catchment, which are more common in published studies, a micro perspective at the pixel level is provided in this study to investigate the vegetation fractional coverage dynamics and build the correlations between vegetation fractional coverage and its multiple influential factors, including precipitation, temperature, soil water, groundwater and human activities in a desert steppe region in the Inner Mongolia Autonomous Region, China. The average vegetation fractional coverage in August for the years 2000–2011 is 0.38 in the study area. The interaction of rain ($R = 0.80$) and heat ($R = -0.76$) significantly determines the growth and distribution of the vegetation in the study area. Besides, the effects of some other factors on vegetation fractional coverage should not be neglected, including groundwater ($R = 0.04$), available water content of soil ($R = 0.23$) and livestock density ($R = 0.28$). From the perspective of centre dynamics for the years 2000–2011, the annual precipitation centre has better synchronism with the vegetation centre, while the movement of the temperature centre is more stable.

Keywords: vegetation fractional coverage; influential factors; Pixel-level; correlation coefficient; desert steppe

1. Introduction

As a consequence of global climate change and human utilization, a large portion of arid and semi-arid ecosystems is either severely altered or on the verge of desertification [1]. Desert steppe is particularly vulnerable, among these ecosystems, as the transition zone from steppe to desert, and its important contributions to ecological stability, global change and food security are widely recognized [2,3]. The desert steppe of Inner Mongolia occupies approximately 18% of the total steppe area in China [3,4]. As a major sandstorm source in north-western China [5], the ecosystems of these regions are very vulnerable for the following main reasons: (1) precipitation, as the main limiting factor of vegetation growth in arid/semi-arid regions, is low and highly variable in amount

and distribution [6,7], characterized by precipitation pulses [8]; (2) strong evaporation and surface radiation exacerbate the water-sensitivity of vegetation in desert steppe [9–11]; (3) the dominant zonal vegetation is herbaceous plants with shallow roots, which have a weak self-sustaining ability and are extremely sensitive to environmental conditions [12,13]; (4) deeply situated in the hinterland of the Eurasian continent, the ecosystem is particularly fragile due to the relatively high altitude and continental climate [14]; (5) with limited ecological capacity, the ecosystem is very susceptible to disturbance from unreasonable human activities such as overgrazing and over-cultivation [15,16]. Therefore, analysing the vegetation dynamics in the desert steppe, and identifying its dominant factors under the impacts of climate change and human activities, is crucial and meaningful for improving the understanding of desertification and taking targeted measures in ecological restoration [17,18].

The Normalized Difference Vegetation Index (NDVI), which uses the Red and Near Infrared spectral bands, can be explicitly related to vegetation productivity [19–22]. The main research directions on NDVI can be summarized as monitoring vegetation dynamics or land cover [23–25], analysing its response with respect to climate change or human activities [26–28], the processing and analysis of NDVI datasets [29–31], and using NDVI for classification or evaluation [32,33]. In contrast to the intensively studied Tibetan Plateau [34–36] or Loess Plateau [37–39], the desert steppe of the Inner Mongolia Autonomous Region receives much less public attention despite also being an ecologically fragile area in Western China. It is vital to determine the influential factors of vegetation growth in desert steppes and understand their respective roles in vegetation dynamics against a backdrop of climate change and human activities. In these types of studies, most focus mainly on precipitation, temperature or human activities, while few combine different factors together, including soil water and groundwater, for an overall discussion and comparison. In addition, a large spatial scale, such as a region or a whole catchment, is more common in published studies. Microscopic view, the pixel level, for example, is seldom discussed.

The objectives of this study are therefore (i) to analyse the spatiotemporal variation of vegetation fractional coverage (VFC) in Darhan Muminggan Joint Banner, a desert steppe region in the Inner Mongolia Autonomous Region, China; (ii) to investigate the correlations between VFC and its multiple influential factors, including precipitation, temperature, soil water, groundwater and human activities at the pixel level; (iii) to identify the dominant factors of VFC. Given that gauging stations in Western China are few and far between [40], Moderate Resolution Imaging Spectroradiometer (MODIS) NDVI and land surface temperature (LST) data, Tropical Rainfall Measuring Mission (TRMM) precipitation data, combined with other measured data, are used for calculation and analysis in this study.

2. Materials and Methods

2.1. Study Area

Darhan Muminggan Joint Banner (DMJB), situated between 41°20′ N~42°40′ N and 109°16′ E~111°25′ E, is a typical border animal husbandry banner in the Midwestern part of the Inner Mongolia Autonomous Region, China. With an average elevation of approximately 1400 m (Figure 1), DMJB has a population of 120,000 spread across an area of 18,200 km². More than 90% (approx. 16,600 km²) of the whole territory is covered by grassland. With a length of 154 km, the Aibugai River is the longest river in DMJB. The river eventually flows into the Tengri Nayur (a lake), which is the lowest altitude in DMJB and almost dry now, due to the construction of water conservancy projects upstream and declining groundwater levels in recent years. Like most rivers in arid/semi-arid regions, the Aibugai River is a seasonal river with limited available water resources [41].
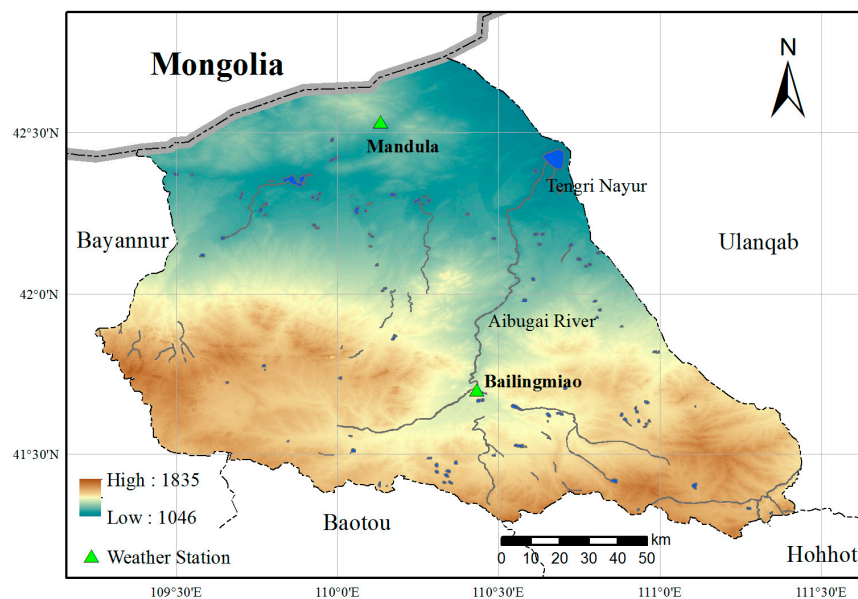
Figure 1. Overview of Darhan Muminggan Joint Banner and locations of weather stations.

With a lack of rainfall and dry all year round, DMJB has climate characteristics typical of a desert steppe region. Without abundant surface water, precipitation, which can vary strongly in temporal and spatial distribution, is the main water source of local ecosystems. Affected by the humid air masses carried by the southeast monsoon, though weak, DMJB has an annual mean precipitation of 253.45 mm, and most of the limited precipitation is consumed by soil evaporation and plant transpiration to sustain the growth of the zonal vegetation [42]. Despite the overall scarcity of rain, more than 60% of the precipitation is concentrated from June to August; if May and September are included, the percentage is more than 80%. Spatially, the precipitation decreases from the southeast to the northwest of DMJB. The annual mean temperature in DMJB is 4.12 °C; in history, the highest temperature is 38 °C in July, and the lowest highest temperature is −39.4 °C in January. The annual mean water surface evaporation is 2480.57 mm (E601). A remarkable characteristic of DMJB is strong winds, with an average wind speed of 3.2–5.2 m/s; wind erosion can be serious, which accelerates soil and water loss and leads to sandstorm weather.

With a vast territory, DMJB has 14 soil units of the FAO-90 classification system (or the FAO-74 classification system) (Figure 2). Although a diverse type, the physical soil structure in the study area is not ideal, characterized by thin soil layer, coarse texture, and high sand content; with serious wind erosion and desertification, the ecosystem in the study area is very fragile. The most common soils in DMJB are Luvic Calcisols (41.1%), Calcic Kastanozems (23.2%), and Haplic Kastanozems (21.1%). All of these three are typical steppe soils in arid/semi-arid regions [43]. Luvic Calcisols are mainly located in the north of the study area, where the average elevation is lower. Haplic Kastanozems occur in higher elevated areas, mainly in the south of DMJB. Calcic Kastanozems are mainly distributed in the central areas between Luvic Calcisols and Haplic Kastanozems. Some other major soils include Calcaric Arenosols (4.8%), Calcic Gleysols (3.6%), Calcic Planosols (2.1%), and Gleyic Phaeozems (1.9%). The dominant vegetation in the study area is xerophyte species in the family Gramineae, including *Stipa klemenzii*, *Stipa krylovii*, *Cleistogenes songorica*, and *Stipa breviflora*. Other species include *Aneurolepidium chinense*, *Artemisia frigida*, *Achnatherum splendens*, and *Caragana microphylla*. The average height of grasses in the study area is 8–15 cm, the VFC is 30–45%, and the maximal biomass appears in mid- to late August.
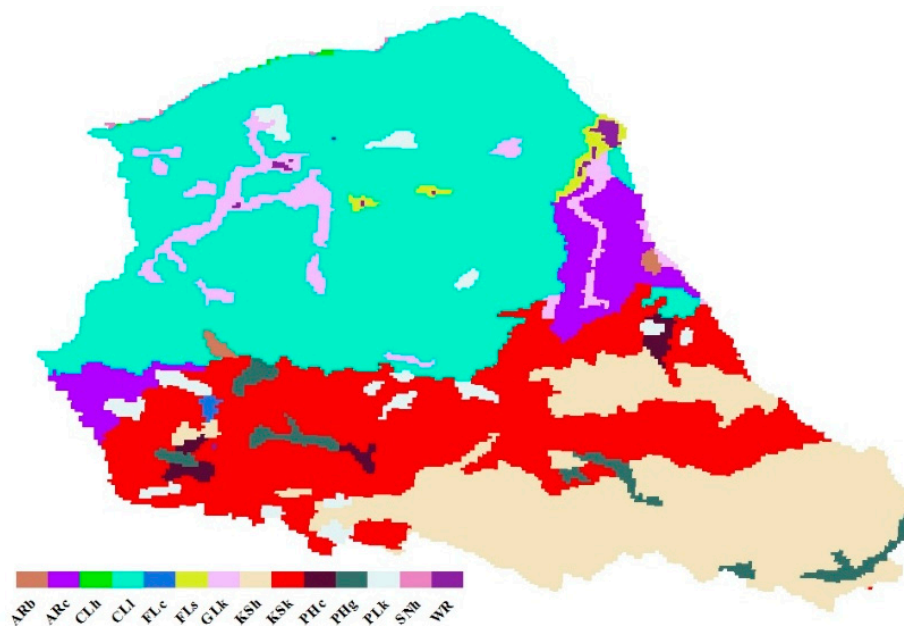
Figure 2. The soil units (FAO-90) in the study area: Cambic Arenosols (ARb); Calcaric Arenosols (ARc); Haplic Calcisols (CLh); Luvic Calcisols (CLl); Calcaric Fluvisols (FLc); Salic Fluvisols (FLs); Calcic Gleysols (GLk); Haplic Kastanozems (KSh); Calcic Kastanozems (KSk); Calcaric Phaeozems (PHc); Gleyic Phaeozems (PHg); Calcic Planosols (PLk); Haplic Solonetz (SNh); Water Regime (WR).

2.2. Data Sources and Processing Methods

In this study, the monthly NDVIs for August from 2000 to 2011 are selected to calculate the annual maximum VFCs; the maximal biomass in the study area appears in mid- to late August, as outlined above. Additionally, the monthly NDVI composites of 500 m are calculated by the MODND1D product via Maximum-Value Composites (MVCs). The NDVI data are then used to calculate the VFC as

$$\text{VFC} = (\text{NDVI} - \text{NDVI}_s) / (\text{NDVI}_v - \text{NDVI}_s) \tag{1}$$

where NDVI_s is the NDVI of bare soil and NDVI_v is the NDVI of the complete coverage of vegetation, which represents the minimum and the maximum NDVI in one area, respectively. In fact, due to the unavoidable clutter interference, the minimum and maximum NDVI in a certain confidence interval are usually chosen as NDVI_s and NDVI_v to reduce noise. In this study, we set a 99% confidence interval, according to the conditions of the images, and pixels with a cumulative probability of pixel values less than 1% and greater than 99% are rejected as noise.

To analyse the correlation between VFC and Land Surface Temperature (LST) of the growing season, we choose the MODIS-LST monthly composites from 2000 to 2011 calculated by the MODLT1T product of 1 km. In addition, since the LST composite comprises day and night LST data, the mean value of day and night LST is computed as the monthly LST. Temperature data, observed by two weather stations in DMJB (Figure 1), are used to test the precision of the MODIS-LST data through correlation analyses during the study period (Figure 3). Both the correlation coefficients between the MODIS-LST data and the observed data exceed 0.96.
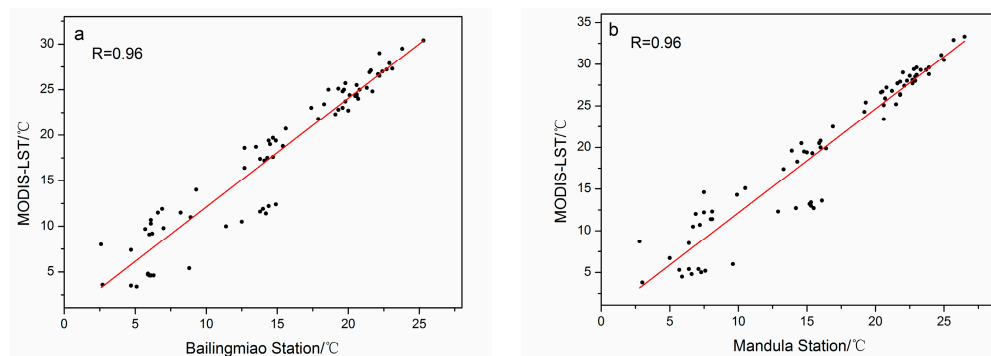
Figure 3. Correlations between the MODIS-LST data and the observed temperature data of Bailingmiao Station (**a**) and Mandula Station (**b**).

The NDVI data and LST data are processed MODIS products in the China region from the TERRA satellite, provided by the International Scientific & Technical Data Mirror Site, Computer Network Information Centre, Chinese Academy of Sciences (http://www.gscloud.cn).

The TRMM is a joint mission between the National Aeronautics and Space Administration (NASA) and the Japan Aerospace Exploration Agency (JAXA) to study rainfall for weather and climate research (http://trmm.gsfc.nasa.gov/). We choose the TRMM 3B43 dataset from 2000 to 2011 to analyse the precipitation impacts on VFC in the study area, at a temporal resolution of a month and spatial resolution of $0.25° × 0.25°$. The precision of TRMM precipitation data are tested by computing the relative error (RE) with the observed precipitation data during the study period (Table 1).

Table 1. The RE between the TRMM precipitation data and the observed precipitation data.

Weather Station	RE/%	
	Monthly Precipitation	Annual Precipitation
Bailingmiao	6.3	2.7
Mandula	−5.6	3.6

Other data include the FAO soil database for soil water parameter calculation, measured groundwater level data from 2010 to 2011, and livestock data from the social and economic statistical yearbooks of DMJB (2000–2011), and village distribution from the first nationwide water resources survey for livestock density calculation.

In this study, all of the spatial data are converted into unified Krasovsky 1940 Albers projected coordinate system and are resampled to grid data with a spatial resolution of 500 m × 500 m. Non-grassland areas are removed to eliminate the effect of other land covers (arable land mainly) on VFC.

2.3. Research Methods

2.3.1. Spatiotemporal Variation of VFC

The grassland in the study area has been divided into low, medium, and high VFC grassland, and their area proportion and variation processes are analysed. The classification standard of the grassland in the study area is as follows (Table 2).

Table 2. The classification of the grassland in the study area.

Classification	Standard and Description
High VFC grassland	Natural and improved grassland with a VFC > 50%, characterized by good growth conditions, and dense grass.
Medium VFC grassland	Natural and improved grassland with a VFC 30–50%, characterized by general growth conditions, sparse grass, and partial visible bare soil.
Low VFC grassland	Natural grassland with a VFC < 30%, characterized by poor growth conditions, obviously sparse grass and apparent bare soil.

In this study, the overall spatiotemporal variation trend of the grassland in the study area from 2000 to 2011 is analysed through the dynamics of the VFC centre. The VFC centre is computed at a pixel level as follows:

$$x_c = \frac{\sum_{i=1}^{m} x_i \cdot C_i}{\sum_{i=1}^{m} C_i} \qquad (2)$$

$$y_c = \frac{\sum_{i=1}^{m} y_i \cdot C_i}{\sum_{i=1}^{m} C_i} \qquad (3)$$

where x_c and y_c are the abscissa and ordinate of the VFC centre; x_i and y_i are the abscissa and ordinate of the ith pixel in the projected coordinate system, respectively; and C_i denotes the VFC of the ith pixel. The dynamics of the VFC centre (x_c and y_c) can reflect the overall spatiotemporal variation trend of the grassland in the study area to some extent.

2.3.2. Correlation Analyses between VFC and Its Influential Factors

For further understanding of the roles of different influential factors in vegetation growth in desert steppe, the correlation coefficients between annual average VFC in the observed years and its influential factors are calculated and analysed at a pixel level, distinct from most previous studies which analysed data at a macroscopic regional scale. All spatial grid data, including VFC and its various influential factors, are converted into point data with pixel information in ArcGIS. The one-to-one correspondence of the extracted point data between the VFC and its influential factors is built in MATLAB by a minimum distance optimizing method within a pixel scale (<500 m). In the next step, the correlation coefficient between VFC and its influential factors is analysed by computing the Pearson correlation coefficient with the formula below:

$$r = \frac{\sum_i (x_i - \overline{x})(y_i - \overline{y})}{\sqrt{\sum_i (x_i - \overline{x})^2 (y_i - \overline{y})^2}} \qquad (4)$$

where x_i and y_i are the independent and dependent variables in the sample, respectively; and $\overline{x}$ and $\overline{y}$ are the sample means.

The influential factors selected for correlation analyses include precipitation, temperature, groundwater, soil water, and human activity.

Precipitation

The significance of precipitation in the ecological processes of arid and semi-arid areas is widely recognized [44,45]. In this study, the pixel-based correlations between VFC and annual precipitation, accumulated precipitation in the non-growing season (November to March including rainfall and snowfall), and monthly precipitation of the growing season (April to October) are analysed. The precipitation data used for analysis are TRMM data, and both the VFC and precipitation data are annual average values from 2000 to 2011.

Temperature

Unlike precipitation, which is positively associated with vegetation growth in most cases, temperature, another crucial role for vegetation growth in arid/semi-arid region, shows different correlations in different cases, which can be either positive or negative [46–48]. The correlations between VFC and monthly temperature of the growing season and effective annual accumulated temperature ($\geq$10 °C) are analysed at a pixel level. The monthly temperature data are from MODIS LST data, and the effective accumulated temperature data are calculated by a 5-day moving average algorithm, using the daily mean temperature data observed by 7 meteorological stations in and adjacent to the study area, and then interpolated into raster GRID format by the inverse distance weighted (IDW) method, carried out in ArcGIS. Both the VFC data and temperature data are annual average values from 2000 to 2011.

Groundwater

Published studies on the effects of groundwater on vegetation in arid and semi-arid areas focus mainly on the available moisture of shrubs and trees, which generally have strong and deep roots [49–52]. Herbaceous plants account for the largest proportion in both biomass and distribution in desert steppe, and usually have short roots; however, studies on the relationship between their growth and distribution and groundwater are few and still a matter of controversy [53–56]. In this study, 105 measured data points (approx. uniform distribution) of the groundwater table in the study area, with the depth not deeper than the threshold depth of the phreatic evaporation (approximately 6.3 m), are used to plot the depth contour of the groundwater level using the Kriging interpolation method (Figure 4), and the correlation between the VFC and groundwater in the study area is then analysed at a pixel level.
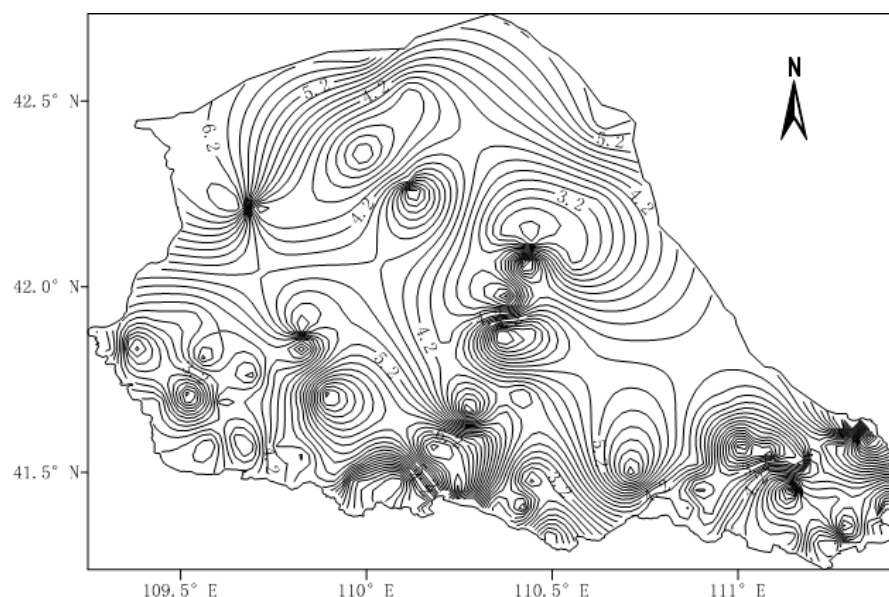

Figure 4. Depth contour of the groundwater level in the study area.

Available Water Content of Soil

Soil water is the direct water source for vegetation during different phonological phases, and soil texture affects vegetation growth and distribution by influencing soil moisture conditions [57–59]. In this study, the available water content (AWC, mmH$_2$O/mm) of soil is selected to analyse its correlation with VFC. The AWC of soil, also known as the available water for vegetation, can

be estimated by calculating the difference between field capacity and the wilting point using the following formula,

$$AWC = FC - WP \tag{5}$$

where AWC is the available water content of soil, vol %; FC is the field capacity, vol %; and WP is the wilting point, vol %. The field capacity and the wilting point of each soil type in the study area are computed by SPAW software (developed by Washington State University, WSU) using the soil mechanical composition parameters in the FAO soil database. The AWC of soil in the study area is transformed into GRID format in ArcGIS (Figure 5).
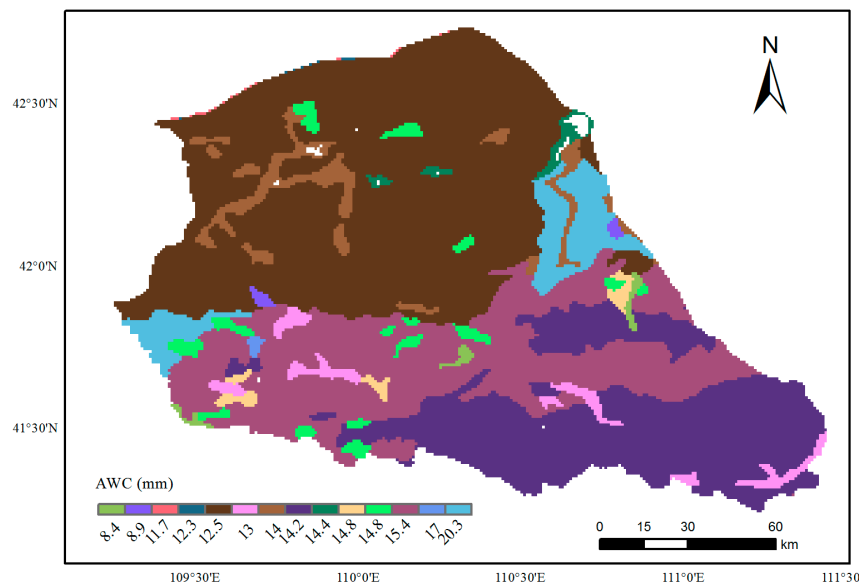

Figure 5. Available water content of soil in the study area.

Human Activities

Overgrazing has been a common and long existing problem in pasture areas of China with the increasing demand for livestock products [60,61]; given that the ecosystem in the desert steppe is more fragile, the effect of overgrazing is more serious [62]. The correlation between VFC and livestock density is analysed to determine the effect of grazing on vegetation distribution. To obtain the GRID data of livestock density in the study area, the large livestock and sheep of each town (the smallest administrative unit of official statistics) are converted into sheep units according to grass consumption, where one large livestock equals five sheep units, and one sheep is one sheep unit. Next, the sheep units of each town are distributed equally into every village of this town with the assumption that the livestock density is high in two cases: (i) a more concentrated village distribution, and (ii) a higher livestock amount. The livestock density distribution map in GRID format is made in ArcGIS using the Kernel Density tool (Figure 6), which can calculate a density from point features using a kernel function to fit a smoothly tapered surface to each point, and the radius of grazing influence is set to 3 km through spot investigation in the study area (the average radius of the 1209 villages in DMJB is 2 km).
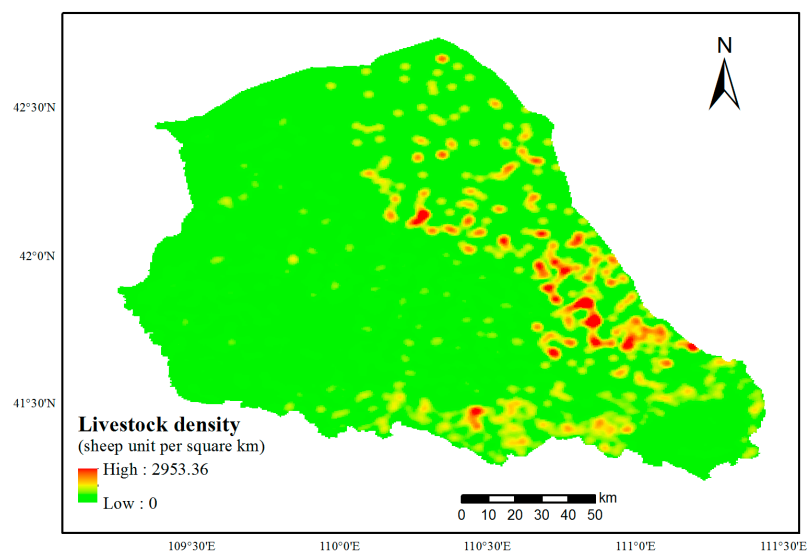
Figure 6. Livestock density distribution in the study area.

2.3.3. Dominant Factor Identification of VFC

By analysing the correlation between VFC and its influential factors, the dominating factors that have a significant effect on the vegetation distribution in the study area are identified, and the response of the spatial and temporal dynamics of the VFC centre to the dominate factors is also analysed at a pixel level.

3. Results and Discussion

3.1. Spatiotemporal Variation of VFC

The average VFC in August for the years 2000–2011 is 0.38 in the study area (Figure 7). A low coefficient of year-to-year VFC variation (ratio of VFC standard deviation to VFC mean) of 12.2% identifies the small temporal variability of the average VFC in the study area for the observed years.
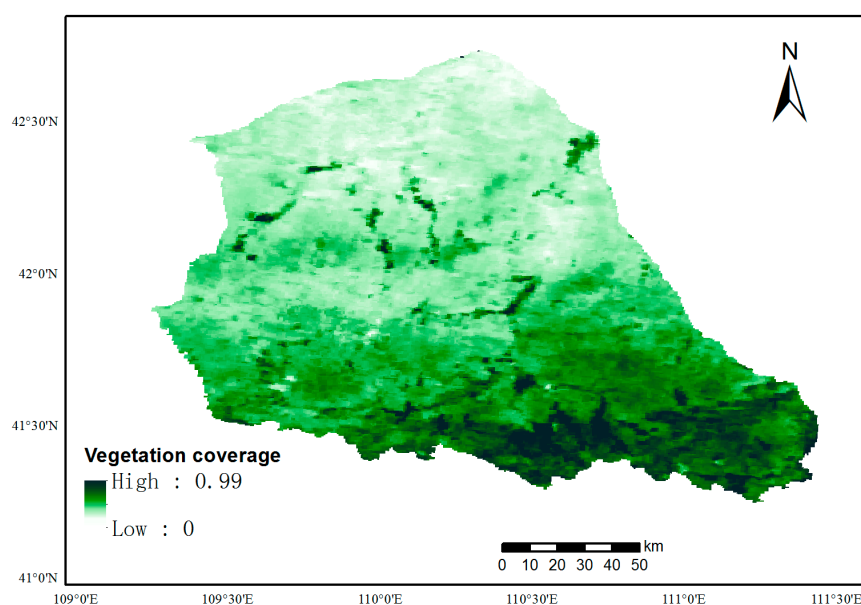

Figure 7. Average VFC in August in the study area for the years 2000–2011.

According to the classification standards of grassland VFC, the annual average area proportion and coefficient of year-to-year area variation (ratio of area standard deviation to area mean, CV_a) during the observed period of the low, medium, and high VFC grassland in the study area are shown in Figure 8. As a desert steppe region, DMJB is dominated by medium-low VFC grassland, accounting for 85.1% of the total area (27.5% and 57.5%, respectively). In terms of the area variation, the low and the high VFC grassland have a much higher coefficient of year-to-year area variation than the medium VFC grassland, which indicates frequent transformation between low and high VFC grassland and the medium VFC grassland.
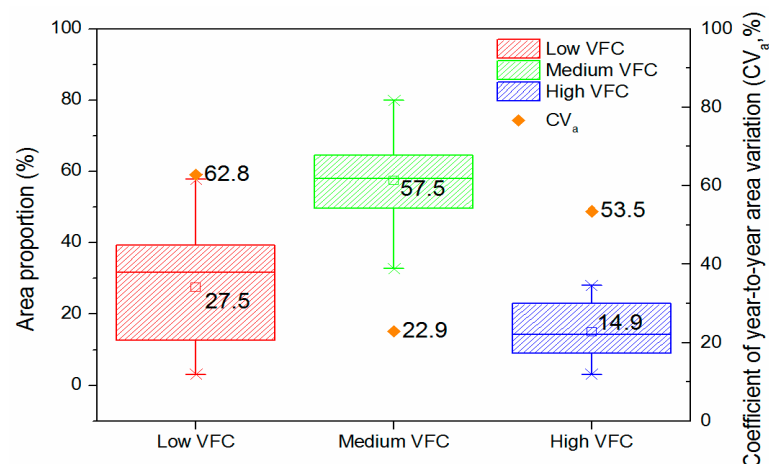

Figure 8. Area proportion and coefficient of year-to-year area variation (CV) of low, medium and high VFC grassland.

Figure 9 shows the spatiotemporal dynamic of the VFC centre in the east-west (Figure 9a) and north-south (Figure 9b) directions. A trend of the VFC centre in the study area moving towards northwest could be observed from the results: 280 m/a westwards and 72 m/a northwards. The dynamic of the VFC centre can reflect the overall variation process of the suitable zone for vegetation growth. Given that DMJB is the transition zone from typical steppe to desert located in the midwestern part of Inner Mongolia, the growth conditions in the southeast of the study area are better than those in the northwest in general; from this view, the possible trend of the VFC centre of the study area moving towards northwest in the observed period could be significant in some research fields, such as desertification and climate change, which implies the possible variation of the suitable zone for vegetation growth in the study area.
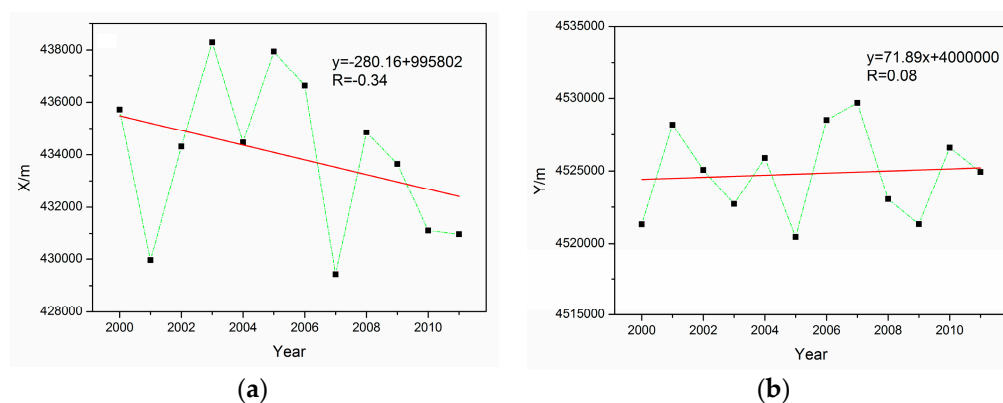

Figure 9. Spatiotemporal dynamic of the VFC centre in the east-west direction (**a**) and north-south direction (**b**).

3.2. Correlation Analysis of the VFC and Its Influential Factors

3.2.1. Precipitation

The correlation coefficients between VFC and monthly precipitation are shown in Table 3; the annual correlation coefficient is 0.8, the annual highest correlation coefficient of 0.79 occurs in the non-growing season (November to March), and July, August, October, and June have correlation coefficients exceeding 0.70. The precipitation process could be divided into three stages to analyse its correlation with vegetation growth, which is the vigorous growth stage from June to August, the decreasing stage including September, October and the non-growing season, and early growth stage including April and May. The rainfall in the vigorous growth stage accounts for more than 60% of the annual precipitation in the study area. With all their correlation coefficients greater than 0.70, the significance of the precipitation from June to August with respect to the growth and distribution of vegetation in desert steppe is obvious. July possesses the highest correlation coefficient (0.78) among these three months. Small in amount, but great in ecological significance, with a proportion of precipitation less than 30%, the precipitation of the decreasing stage has a strong correlation with VFC. In particular, the precipitation of the five months in the non-growing season from November to March (most of which is snowfall), which only accounts for 8.6% of annual precipitation, has the very impressive correlation coefficient of 0.79, even greater than that of July, which demonstrates the snowfall in the non-growing season may have important impacts on VFC in desert steppe. The rainfall in the early growth stage is low, with the proportion less than 12%, the correlation with VFC is weak as well. The vegetation in desert steppe is becoming green in this stage with relatively weaker physiological activities, the water demand in this period is limited; thus, in addition, the soil water remaining in the non-growing season seems to play an important role, which reveals that the rainfall and snowfall before the early growth stage may weaken the effect of precipitation in this stage on VFC.

Table 3. Precipitation proportion and the correlation coefficients between precipitation and VFC.

Period	Precipitation (mm)	Proportion (%)	Correlation Coefficient
Non-growing season	18.99	8.6	0.79
April	48.78	3.3	0.47
May	48.22	8.5	0.38
June	10.60	16.7	0.7
July	36.70	22.2	0.78
August	30.60	21.9	0.75
September	7.33	13.9	0.65
October	18.63	4.8	0.75
Annual	219.85	100	0.8

3.2.2. Temperature

The correlation coefficients between VFC and effective annual accumulated temperature (≥ 10 °C), monthly temperature in the growth season (April to October), and average temperature in the growth season are shown in Table 4.

Table 4. The correlation coefficients between VFC and temperature in the study area.

Period	Correlation Coefficient
Annual accumulated temperature ≥ 10 °C	−0.36
April	−0.62
May	−0.68
June	−0.71
July	−0.78
August	−0.82
September	−0.77
October	−0.58
Growing season	−0.76

Two main conclusions can be drawn from the results: (1) temperature is negatively associated with the growth and distribution of vegetation in the study area; and (2) the correlation coefficients are generally high.

Given the rare rainfall in the desert steppe, both of the above results could be analysed associated with precipitation in the corresponding period. Evapotranspiration, directly related to temperature, affects vegetation growth by affecting soil water distribution, which in turn supplies the direct water source to most shallow-root vegetation. Similar to precipitation, the temperature of the vigorous growth stage from June to August shows very strong correlations with VFC, albeit negatively. The effect of rain and heat appearing at the same time seems to aggravate the ecological vulnerability in the desert steppe; once the rainfall in the vigorous growth stage is insufficient, a sharp decrease in biomass seems inevitable, considering that herbaceous plants with poor self-sustaining abilities depend strongly on soil water of the root zone.

As for September and October in the decreasing stage, the influence of temperature on vegetation growth emerges in the next growing season by affecting the storage of soil water by evapotranspiration. With more rainfall and higher temperatures, the correlation coefficient of September is obviously greater than October.

In terms of the effective annual accumulated temperature (≥ 10 °C), the correlation coefficient of -0.36 reveals that the influence of accumulated temperature is not that significant when compared with temperature, considering that the sunshine in the desert steppe is sufficient.

3.2.3. Groundwater

The correlation coefficient between vegetation and groundwater is only 0.04. Generally, precipitation and groundwater are considered to be the two main water sources for vegetation growth. Groundwater is especially important for some shrubs and trees, which have deep and strong roots in some arid/semi-arid regions. For the herbaceous plants with shallow roots no deeper than 1 m (most of them are not deeper than 40–50 cm in the study area), the phreatic evaporation is also believed to be available for some vegetation. Our study analyses the correlation between VFC and groundwater at a pixel level, and shows that the effect of groundwater on VFC is not that significant compared to precipitation and temperature. However, the weak correlation does not mean that the groundwater is meaningless to vegetation growth; it just indicates that the effect of groundwater on determining the spatial distribution of vegetation is far less than that of precipitation and temperature, as far as the whole study area is concerned.

3.2.4. Available Water Content of Soil

The correlation coefficient between vegetation and available water content of soil is 0.23. The available water content of soil reflects the water storage capacity of soil; under the same conditions, soil with higher available water content can provide more available water for vegetation growth. However, this capacity is also limited by multiple factors, such as the strong evaporation of soil water in desert steppe. From the spatial scale of the whole study area, the available water content of soil affects the distribution of vegetation to some extent, but not as much as precipitation and temperature.

3.2.5. Livestock Density

In recent decades, the increasing influences of human activities on the various ecosystems have caused more and more concerns. Overgrazing is thought to be one of the most serious effects of human activities on grassland ecosystems. The VFC is significantly positively ($p < 0.01$) associated with the livestock density, with a correlation coefficient of 0.28. This result demonstrates that the influence of human activities in the study area is even greater than some natural factors formed over a long time, such as groundwater and soil water.

3.3. Spatiotemporal Analyses of the Dominant Factors

Precipitation and temperature are the two dominant factors of VFC in the study area through the correlation analyses above (Figure 10).
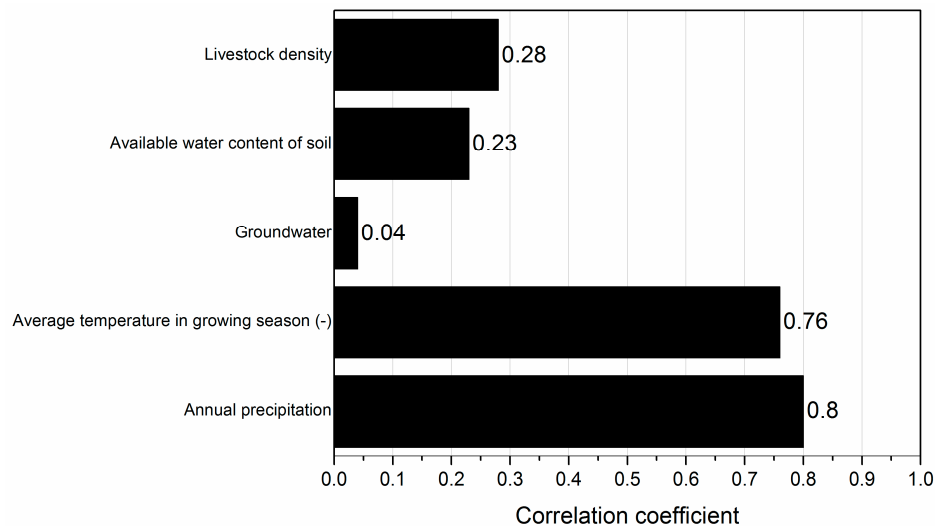

Figure 10. Correlation coefficients of the influential factors of VFC in the study area.

In the previous analyses, we discuss the dynamics of the VFC centre in the study area. Next, the dynamics of precipitation and temperature centres, together with that of the VFC centre, are shown in Figure 11 for comparing their moving trend. The annual precipitation centre has better synchronism with the VFC centre, as they have almost the same moving trend in the observed period, while the movement of the temperature centre is more stable. Annually and seasonally, precipitation in this arid/semi-arid region displays very strong pulse dynamic characteristics, which can trigger various ecological processes. The VFC centre dynamics in the study area are affected mainly by precipitation processes.
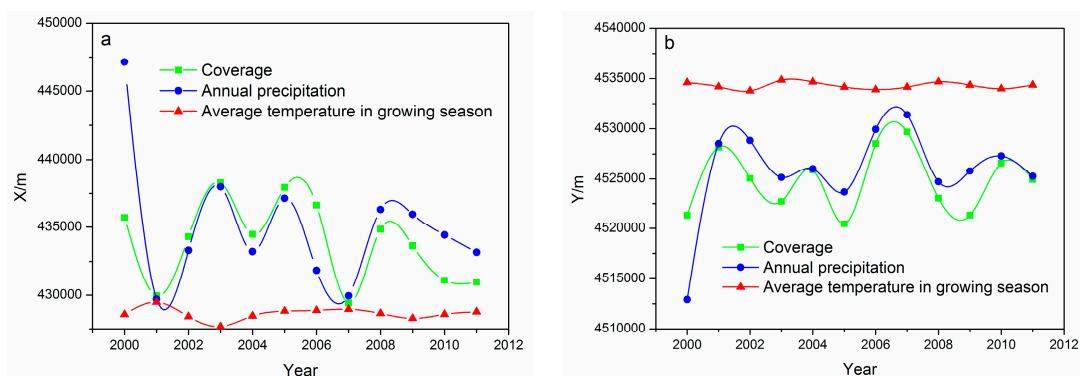

Figure 11. Dynamics of precipitation, temperature and VFC centres in the east-west direction (**a**) and north-south direction (**b**) in the study area from 2000 to 2011.

4. Conclusions

In this study, the spatiotemporal variations of VFC, and the correlations between VFC and its influential factors in DMJB, are analysed at the pixel level, and the dominant factors of the desert steppe are further identified and discussed. The interaction of rain and heat significantly determines the growth and distribution of the vegetation of the desert steppe in the study area, and the effects of some other factors, especially overgrazing, should not be ignored.

The main conclusions of this study are as follows:

(1) The average VFC in August for the years 2000–2011 is 0.38 in the study area, with a low coefficient of year-to-year VFC variation of 12.2%. The study area is dominated by medium-low VFC grassland with an area proportion of 85.1%. A northwest moving trend of the VFC centre is evident in the observed period at a speed of 280 m/a westwards and 72 m/a northwards.

(2) The correlation coefficient between VFC and annual precipitation is 0.80 in the observed period. The non-growing season (November to March), July, August, October, and June have correlation coefficients greater than 0.70, and the highest correlation coefficient of 0.79 occurred in the non-growing season.

(3) Under the influence of evapotranspiration, temperature is negatively associated with VFC in the study area. The correlation coefficient between VFC and the average temperature in the growing season is -0.76, while the correlation coefficient between VFC and effective annual accumulated temperature (≥ 10 °C) is -0.36.

(4) The correlations between VFC and ground water, the available water content of soil, and the livestock density are not that significant compared to precipitation and temperature in the study area, with correlation coefficients of 0.04, 0.23, and 0.28, respectively. Continued attention should be paid to the impact of overgrazing on desert steppe.

(5) The dominant factors of the VFC in the study area are precipitation and temperature. From the perspective of centre dynamics for the years 2000–2011, the annual precipitation centre has better synchronism with the VFC centre, while the movement of temperature centre is more stable, which reveals that the dynamics of the VFC centre are mainly affected by precipitation in the observed years.

Pixel-level spatiotemporal analyses of VFC variation and its influential factors provide a unique perspective to survey the vegetation dynamics in a desert steppe. By building the links between VFC and its influential factors based on a large amount of pixel information, some easily ignored facts are described quantitatively. For example, although the meaning of non-growing season precipitation in arid/semi-arid regions is sometimes discussed, its effect may still be underestimated, at least in statistics, by correlation analysis at a pixel scale.

Author Contributions: Yifan Song performed the statistical analyses and wrote the paper. Zhongxiao Guo and Denghua Yan helped revise the paper. Yajing Lu helped with language editing and some data analyses. Zilong Liao, Yingjie Cui and Huiwen Liu helped in data collecting and processing.

Conflicts of Interest: The authors declare no conflict of interest.

References

1. Schlesinger, W.H.; Reynolds, J.F.; Cunningham, G.L.; Huenneke, L.F.; Jarrell, W.M.; Virginia, R.A.; Whitford, W.G. Biological feedbacks in global desertification. *Science* **1990**, *247*, 1043–1048. [CrossRef] [PubMed]

2. Zhan, X.; Li, L.; Cheng, W. Restoration of Stipa kryloviisteppes in Inner Mongolia of China: Assesment of seed banks and vegetation composition. *J. Arid Environ.* **2007**, *68*, 298–307. [CrossRef]

3. Fang, J.; Bai, Y.; Li, L.; Jiang, G.; Huang, J.; Huang, Z.; Zhang, W.; Gao, S. Scientific basis and practical ways for sustainable development of China's pasture regions. *Chin. Sci. Bull.* **2016**, *61*, 155–164. (In Chinese)

4. Liao, G. *Grassland Resource of China*; Chinese Science and Technology Publisher: Beijing, China, 1996. (In Chinese)

5. Yang, X.; Xu, B.; Jin, Y.; Qin, Z.; Ma, H.; Li, J.; Zhao, F.; Chen, S.; Zhu, X. Remote sensing monitoring of grassland vegetation growth in the Beijing–Tianjin sandstorm source project area from 2000 to 2010. *Ecol. Indic.* **2015**, *51*, 244–251. [CrossRef]

6. Noy-Meir, I. Desert ecosystems: Environment and producers. *Ann. Rev. Ecol. Syst.* **1973**, *4*, 25–52. [CrossRef]

7.　Bailey, H.P. Semi-Arid Climates: Their Definition and Distribution. *Agric. Semi-Arid Environ.* **1979**, *34*, 73–97.

8.　Cable, J.; Huxman, T. Precipitation pulse size effects on Sonoran Desert soil microbial crusts. *Oecologia* **2004**, *141*, 317–324. [CrossRef] [PubMed]

9.　Jung, M.; Reichstein, M.; Ciais, P.; Seneviratne, S.I.; Sheffield, J.; Goulden, M.L.; Bonan, G.; Cescatti, A.; Chen, J.; de Jeu, R.; et al. Recent decline in the global land evapotranspiration trend due to limited moisture supply. *Nature* **2010**, *467*, 951–954. [CrossRef] [PubMed]

10.　Armstrong, R.; Pomeroy, J.; Martz, L. Variability in evaporation across the Canadian Prairie region during drought and non-drought periods. *J. Hydrol.* **2015**, *521*, 182–195. [CrossRef]

11.　Bittellia, M.; Ventura, F.; Campbell, G.S.; Snyder, R.L.; Gallegati, F.; Pisa, P.R. Coupling of heat, water vapor, and liquid water fluxes to compute evaporation in bare soils. *J. Hydrol.* **2008**, *362*, 191–205. [CrossRef]

12.　Li, F.; Zhao, W.; Liu, H. The Response of Aboveground Net Primary Productivity of Desert Vegetation to Rainfall Pulse in the Temperate Desert Region of Northwest China. *PLoS ONE* **2013**, *8*, e73003. [CrossRef] [PubMed]

13.　Chu, C.; Havstad, K.; Kaplan, N.; Lauenroth, W.; McClaran, M.; Peters, D.; Vermeire, L.; Adler, P.; Rapson, G. Life form influences survivorship patterns for 109 herbaceous perennials from six semi-arid ecosystems. *J. Veg. Sci.* **2014**, *25*, 947–954. [CrossRef]

14.　Jiang, W.; Guo, Z.; Sun, X.; Wu, H.; Chu, G.; Yuan, B.; Hatté, C.; Guiot, J. Reconstruction of climate and vegetation changes of Lake Bayanchagan (Inner Mongolia): Holocene variability of the East Asian monsoon. *Quat. Res.* **2006**, *65*, 411–420. [CrossRef]

15.　Feng, Q.; Ma, H.; Jiang, X.; Wang, X.; Cao, S. What Has Caused Desertification in China? *Sci. Rep. UK* **2015**. [CrossRef] [PubMed]

16.　Zhu, G.; Deng, L.; Zhang, X.; Shangguan, Z. Effects of grazing exclusion on plant community and soil physicochemical properties in a desert steppe on the Loess Plateau, China. *Ecol. Eng.* **2016**, *90*, 372–381. [CrossRef]

17.　Runnström, M.C. Is Northern China Winning the Battle against Desertification? *AMBIO J. Hum. Environ.* **2009**, *29*, 468–476. [CrossRef]

18.　Cao, S. Impact of China's Large-Scale Ecological Restoration Program on the Environment and Society in Arid and Semiarid Areas of China: Achievements, Problems, Synthesis, and Applications. *Crit. Rev. Environ. Sci. Techonol.* **2011**, *41*, 317–335. [CrossRef]

19.　Carlson, T.; Ripley, D. On the relation between NDVI, fractional vegetation cover, and leaf area index. *Remote Sens. Environ.* **1997**, *62*, 241–252. [CrossRef]

20.　Sellers, P.J.; Tucker, C.J.; Collatz, G.J.; Los, S.O.; Justice, C.O.; Dazlich, D.A.; Randall, D.A. A global 1° by 1° NDVI data set for climate studies. Part 2: The generation of global fields of terrestrial biophysical parameters from the NDVI. *Int. J. Remote Sens.* **1994**, *15*, 3519–3545. [CrossRef]

21.　Valor, E.; Caselles, V. Mapping land surface emissivity from NDVI: Application to European, African, and South American areas. *Remote Sens. Environ.* **1996**, *57*, 167–184. [CrossRef]

22.　Eckert, S.; Hüsler, F.; Liniger, H.; Hodel, E. Trend analysis of MODIS NDVI time series for detecting land degradation and regeneration in Mongolia. *J. Arid Environ.* **2015**, *113*, 16–28. [CrossRef]

23.　Cai, D.; Fraedrich, K.; Sielmann, F.; Guan, Y.; Guo, S.; Zhang, L.; Zhu, X. Climate and Vegetation: An ERA-Interim and GIMMS NDVI Analysis. *J. Clim.* **2014**, *27*, 5111–5118. [CrossRef]

24.　Cai, D.; Fraedrich, K.; Sielmann, F.; Zhang, L.; Zhu, X.; Guo, S.; Guan, Y. Vegetation Dynamics on the Tietan Plateau (1982–2006): An Attribution by Ecohydrological Diagnostics. *J. Clim.* **2015**, *28*, 4576–4584. [CrossRef]

25.　Detsch, F.; Otte, I.; Appelhans, T.; Hemp, A.; Nauss, T. Seasonal and long-term vegetation dynamics from 1-km GIMMS-based NDVI times series at Mt. Kilimanjaro, Tanzania. *Remote Sen. Environ.* **2016**, *178*, 70–83. [CrossRef]

26.　Green, S.; Cawkwell, F.; Dwyer, E. Cattle stocking rates estimated in temperate intensive grasslands with a spring growth model derived from MODIS NDVI time-series. *Int. J. Appl. Earth Obs. Geoinf.* **2016**, *52*, 166–174. [CrossRef]

27.　Pettorelli, N.; Vik, J.; Mysterud, A.; Gaillard, J.; Tucker, C.; Stenseth, N. Using the satellite-derived NDVI to assess ecological responses to environmental change. *Trends Ecol. Evol.* **2005**, *20*, 503–510. [CrossRef] [PubMed]

28.　Sen, I. AVHRR-NDVI-based crop coefficients for analyzing long-term trends in evapotranspiration in relation to changing climate in the U.S. High Plains. *Water Resour. Res.* **2013**, *49*, 231–244.

29. Tucker, C.J.; Pinzon, J.E.; Brown, M.E.; Slayback, D.A.; Pak, E.W.; Mahoney, R.; Vermote, E.F.; Saleous, N.E. An extended AVHRR 8-km NDVI dataset compatible with MODIS and SPOT vegetation NDVI data. *Int. J. Remote Sens.* **2005**, *26*, 4485–4498. [CrossRef]

30. Chen, J.; Jönsson, P.; Tamura, M.; Gu, Z.; Matsushita, B.; Eklundh, L. A simple method for reconstructing a high-quality NDVI time-series data set based on the Savitzky–Golay filter. *Remote Sens. Environ.* **2004**, *91*, 332–344. [CrossRef]

31. Tian, F.; Fensholt, R.; Verbesselt, J.; Grogan, K.; Horion, S.; Wang, Y. Evaluating temporal consistency of long-term global NDVI datasets for trend analysis. *Remote Sens. Environ.* **2015**, *163*, 326–340. [CrossRef]

32. Defries, R.S.; Townshend, J.R.G. NDVI-derived land cover classifications at a global scale. *Int. J. Remote Sens.* **1994**, *15*, 3567–3586. [CrossRef]

33. Park, J.; Ahn, S.; Hwang, S.; Jang, C.; Park, G.; Kim, S. Evaluation of MODIS NDVI and LST for indicating soil moisture of forest areas based on SWAT modeling. *Paddy Water Environ.* **2014**, *12*, 77–88. [CrossRef]

34. Liu, X.; Chen, B. Climatic warming in the Tibetan plateau during recent decades. *Int. J. Climatol.* **2000**, *20*, 1729–1742. [CrossRef]

35. Royden, L.; Burchfiel, B.; van der Hilst, R.D. The geological evolution of the Tibetan Plateau. *Science* **2008**, *321*, 1054–1058. [CrossRef] [PubMed]

36. Gao, Y.; Li, X.; Leung, L.; Chen, D.; Xu, J. Aridity changes in the Tibetan Plateau in a warming climate. *Environ. Res. Lett.* **2015**, *10*, 34013–34024. [CrossRef]

37. An, Z.; Kukla, G.; Porter, S.; Xiao, J. Magnetic susceptibility evidence of monsoon variation on the Loess Plateau of central China during the last 130,000 years. *Quat. Res.* **1991**, *36*, 29–36. [CrossRef]

38. Fu, B.; Chen, L.; Ma, K.; Zhou, H.; Wang, J. The relationships between land use and soil conditions in the hilly area of the loess plateau in northern Shaanxi, China. *Catena* **2000**, *39*, 69–78. [CrossRef]

39. Boegman, L.; Ivey, G.; Imberger, J. Modeling soil–water dynamics and soil–water carrying capacity for vegetation on the Loess Plateau, China. *Agric. Water Manag.* **2015**, *159*, 176–184.

40. He, H. China gauging station network. *Adv. Water Sci.* **2010**, *21*, 460–465.

41. Mujumdar, P.; Sasikumar, K. A fuzzy risk approach for seasonal water quality management of a river system. *Water Resour. Res.* **2002**, *38*. [CrossRef]

42. Wang, F.; Liang, R.; Yang, X.; Chen, M. A study of ecological water requirements in northwest China I: Theoretical analysis. *J. Nat. Resour.* **2002**, *17*, 1–8. (In Chinese)

43. Schaffrath, D.; Barthold, F.; Bernhofer, C.; Milchunas, D.; Lauenroth, W.; Chapman, P.; Kazempour, M. Effects of grazing, topography, and precipitation on the structure of a semiarid grassland. *Plant Ecol.* **1989**, *80*, 11–23.

44. Le, H.; Bingham, R.; Skerbek, W. Relationship between the variability of primary production and the variability of annual precipitation in world arid lands. *J. Arid Environ.* **1988**, 1–18. [CrossRef]

45. Zhou, J.; Fu, B.; Gao, G.; Lü, Y.; Liu, Y.; Lü, N.; Wang, S. Effects of precipitation and restoration vegetation on soil erosion in a semi-arid environment in the Loess Plateau, China. *Catena* **2016**, *137*, 1–11. [CrossRef]

46. Piao, S.; Mohammat, A.; Fang, J.; Cai, Q.; Feng, J. NDVI-based increase in growth of temperate grasslands and its responses to climate changes in China. *Glob. Environ. Chang.* **2006**, *16*, 340–348. [CrossRef]

47. Xu, W.; Gu, S.; Zhao, X.; Xiao, J.; Tang, Y.; Fang, J.; Zhang, J.; Jiang, S. High positive correlation between soil temperature and NDVI from 1982 to 2006 in alpine meadow of the Three-River Source Region on the Qinghai-Tibetan Plateau. *Int. J. Appl. Earth Obs. Geoinform.* **2011**, *13*, 528–535. [CrossRef]

48. Lei, L.; Tashpolat, T.; Li, J.; Zhang, F.; Tian, Y. Correlation between Land Surface Temperature and Vegetation Coverage in a Typical Arid Oasis. *J. Desert Res.* **2011**, *31*, 1001–1007. (In Chinese)

49. Kizito, F.; Dragila, M.; Sène, M.; Lufafa, A.; Diedhiou, I.; Dick, R.; Selker, J.; Dossa, E.; Khouma, M.; Badiane, A.; et al. Seasonal soil water variation and root patterns between two semi-arid shrubs co-existing with Pearl millet in Senegal, West Africa. *J. Arid Environ.* **2006**, *67*, 436–455. [CrossRef]

50. Jacobsen, A.; Pratt, R.; Davis, S.; Ewers, F. Cavitation resistance and seasonal hydraulics differ among three arid Californian plant communities. *Plant Cell Environ.* **2007**, *30*, 1599–1609. [CrossRef] [PubMed]

51. Jacobsen, A.; Pratt, B.; Davis, S.; Ewers, F. Comparative community physiology: Nonconvergence in water relations among three semi-arid shrub communities. *New Phytol.* **2008**, *180*, 100–113. [CrossRef] [PubMed]

52. Wang, X.; Wang, Z.; Berndtsson, R.; Zhang, Y.; Pan, Y. Desert shrub stemflow and its significance in soil moisture replenishment. *Hydrol. Earth Syst. Sci.* **2011**, *15*, 561–567. [CrossRef]

53. Cooper, D.J.; Sanderson, J.S.; Stannard, D.I.; Groeneveld, D.P. Effects of long-term water table drawdown on evapotranspiration and vegetation in an arid region phreatophyte community. *J. Hydrol.* **2006**, *325*, 21–34. [CrossRef]

54. Kløve, B.; Ala-Aho, P.; Bertrand, G.; Boukalova, Z.; Ertürk, A.; Goldscheider, N.; Ilmonen, J. Groundwater dependent ecosystems. Part I: Hydroecological status and trends. *Environ. Sci. Policy* **2011**, *14*, 770–781. [CrossRef]

55. Fan, Y. Groudwater in the Earth's critical zone: Relevance to large-scale patterns and processes. *Water Resour. Res.* **2015**, *51*, 3052–3069. [CrossRef]

56. Ghamarnia, H.; Khodaei, E. Evidence on shallow groundwater use by edible green vegetables such as *Solanum pseudoca psicum*, *Ocimum basilicum* and *Lepidium sativum* in a semi-arid climate condition. *Agric. Water Manag.* **2016**, *165*, 198–210. [CrossRef]

57. Wildung, R.; Garland, T.; Buschbom, R. The interdependent effects of soil temperature and water content on soil respiration rate and plant root decomposition in arid grassland soils. *Soil Biol. Biochem.* **1975**, *7*, 373–378. [CrossRef]

58. Allison, G.; Hughes, M. The use of natural tracers as indicators of soil-water movement in a temperate semi-arid region. *J. Hydrol.* **1983**, *60*, 157–173. [CrossRef]

59. Gómez-Plaza, A.; MartíNez-Mena, M.; Albaladejo, J.; Castillo, V. Factors regulating spatial distribution of soil water content in small semiarid catchments. *J. Hydrol.* **2001**, *253*, 211–226. [CrossRef]

60. Pei, S.; Fu, H.; Wan, C. Changes in soil properties and vegetation following exclosure and grazing in degraded Alxa desert steppe of Inner Mongolia, China. *Agric. Ecosyst. Environ.* **2008**, *124*, 33–39. [CrossRef]

61. Rong, Y.; Yuan, F.; Ma, L. Effectiveness of exclosures for restoring soils and vegetation degraded by overgrazing in the Junggar Basin, China. *Grassl. Sci.* **2014**, *60*, 118–124. [CrossRef]

62. Unkovich, M.; Nan, Z. Problems and prospects of grassland agroecosystems in western China. *Agric. Ecosyst. Environ.* **2008**, *124*, 1–2. [CrossRef]